THERMALLY ACTIVATED SERPENTINE LEACHING UNDER FLUE GAS CONDITIONS IN A BUBBLE COLUMN REACTOR OPERATED AT AMBIENT PRESSURE AND TEMPERATURE

Ilies Tebbiche[*], Louis-César Pasquier[*], Guy Mercier[*], Jean-Francois Blais[*], Sandra Kentish[**]

*Institut National de la Recherche Scientifique (Centre Eau, Terre et Environnement), Université du Québec, 490 rue de la Couronne, Quebec, Quebec G1K 9A9, Canada

** Department of Chemical and Biomolecular Engineering, The University of Melbourne, Parkville, Victoria 3010, Australia

HIGHLIGHTS

- Activated serpentine leaching under flue gas CO_2 concentrations.
- 32 % Mg content of activated serpentine recovered into solution
- Mg leaching shown to be limited by silica solubility
- Synergetic effect between CO_2 absorption and activated serpentine leaching

ABSTRACT

Mineral carbonation of serpentine in the aqueous phase traditionally required high temperatures and pressures or additives to dissolve the mineral. This was accompanied by significant costs and important environmental burdens. This paper aims to demonstrate the feasibility of thermally activated serpentine leaching under ambient temperature and pressure. A simulated cement flue gas effluent with a CO_2 content of 18.2 % on a volume basis was used. The reaction was performed in a bubble column operated under a homogeneous regime. Agitation was required to improve solution mixing and CO_2 diffusion.

Results showed that the extent of Mg leaching was limited by the low solubility of silica in the aqueous solution. Once the solution was saturated with silica, CO_2 dissolution acted only to cause precipitation of magnesium carbonate. Successive leaching with fresh water partially limited the problem as serpentine leaching declined with time. A total of 32% of the serpentine magnesium content was recovered from the solution after six successive leaching stages. For comparison, 33% of the content of the same material was dissolved when the reaction was performed in a batch reactor operated under 11.5 bar total pressure. In addition to costs and environmental improvements, these results have positive consequences on reducing complexity and retrofit issues for the application of mineral carbonation with serpentine.

It was also shown that improving CO_2 mass transfer through increasing agitation or superficial gas velocity accelerated serpentine leaching, highlighting the synergistic effect between the two reactions.

Keywords: activated serpentine, bubble column, serpentine leaching, mineral carbonation

1 INTRODUCTION

Mineral carbonation was proposed in the early 90s as a promising solution to tackle CO_2 emission issues (Seifritz, 1990). This reaction occurs when CO_2 is bound chemically to a mineral securing long term storage (Seifritz, 1990). Large anthropogenic CO_2 quantities emitted daily led mineral carbonation research to focus on available and affordable materials (Vitillo, 2015). With an important feedstock volume and moderate reactivity, serpentine was considered a very good candidate (Goff *et al.*, 2000). The global serpentine carbonation reaction is generally referred to by (Eq 1) (Olajire, 2013)

$$\mathrm{Mg_3Si_2O_5(OH)_4}(s) + 3\,CO_2\,(g) \rightarrow 3\,MgCO_3 + 2\,SiO_2 + 2\,H_2O \qquad \text{(Eq 1)}$$

Aqueous phase carbonation under neutral pH and ambient conditions is limited and Mg leaching is generally considered as the reaction-limiting step (Luce *et al.*, 1972; Schulze *et al.*, 2004). As the Mg leaching reaction might suggest (Eq 2), strong acid conditions improve serpentine leaching (Luce *et al.*, 1972):

$$\mathrm{Mg_3Si_2O_5(OH)_4}(s) + 6\mathrm{H^+}(aq) \rightarrow 3\mathrm{Mg^{2+}}(aq) + 2\mathrm{H_4SiO_4}(aq) + 7\mathrm{H_2O}\,(l) \qquad \text{(Eq 2)}$$

The natural serpentine crystalline structure limits access to the Mg atoms which hinders dissolution. Mechanical or thermal activation removes the bound hydroxyl atoms from the mineral brucite group $[Mg_3O_2(OH)_4]^{2-}$ leading to a more reactive amorphous form (Dlugogorski & Balucan, 2014; Gerdemann *et al.*, 2007; Li & Hitch, 2018). However, only a partial removal of the OH^- groups is desired as the total serpentine dehydroxylation leads to the formation of forsterite [Mg_2SiO_4] which is another less reactive crystalline mineral (Balucan, 2013; Balucan *et al.*, 2013).

In regards to CO_2, the leaching process can be described by (Eq 3-5) (Chen *et al.*, 2006). This process is strongly dependent on temperature, p_{CO2} and solution pH: the CO_2 vapor-liquid equilibrium (Eq 3) is enhanced at low temperature and high p_{CO2} while the carbonate and bicarbonate formation (Eq 4-5) is catalyzed under alkaline conditions (Pasquier *et al.*, 2014b; Wang *et al.*, 2010). Reaction conditions leading to low CO_2 concentrations in the liquid phase might lead to CO_2 becoming the reaction-limiting step for the global carbonation reaction (Sipilä *et al.*, 2008).

$$CO_2\ (g) + H_2O\ (l) \leftrightarrow H_2CO_3\ (aq) \quad \text{(Eq 3)}$$

$$H_2CO_3\ (aq)\ \leftrightarrow H^+\ (aq) + HCO_3^-\ (aq) \quad \text{(Eq 4)}$$

$$HCO_3^-\ (aq)\ \leftrightarrow H^+\ (aq) + CO_3^{2-}\ (aq) \quad \text{(Eq 5)}$$

Werner et al. studied dehydroxylated serpentine leaching at both the natural slurry pH (8-9) and acid pH (4-6) for a temperature range of 30-120°C and p_{CO2} ranging from 0.1 to 2 bar (Werner *et al.*, 2014a; Werner *et al.*, 2014b). They confirmed that acidity improved the dissolution of activated serpentine through Eq. 2. Increasing the p_{CO2} had a positive effect on the dissolution as it increased the acidity (Werner *et al.*, 2014a). On the other hand, the temperature had a different effect depending on the pH and solid concentration. Under acid pH and with very dilute slurries (<0.2 wt%), an increase of temperature from 30 to 90°C increased the dissolution extent from 40 to 70% under p_{CO2} = 2 bar after 2 h (Werner *et al.*, 2014b). Under natural pH and with more concentrated slurries (5-20 wt%), the same increase in temperature reduced the leaching efficiency from 32% to 22% for the same reaction time (Werner *et al.*, 2014a). The higher initial solid concentration and higher pH resulted in faster solution saturation in regards to carbonate and silica. Consequently, this accelerated precipitation of magnesium carbonate, leading to the formation of a layer at the solid surface which reduced further diffusion of the Mg resulting in reducing the reaction extent (Werner *et al.*, 2014a). Similar conclusions were made in a more recent study (Farhang *et al.*, 2017). Note that (Eq 1) refer to magnesite as the carbonate formed during the serpentine carbonation while the type of carbonate formed strongly depends on operating conditions (Hänchen *et al.*, 2008). Magnesite formation (Eq 6) can only be obtained at high temperature (≈> 120°C) while hydromagnesite (Eq 7) is formed at average temperature (>60°C) and nesquehonite (Eq 8) is the main form present at ambient to low temperatures (20-60°C) (Hänchen *et al.*, 2008). On the other hand, silica precipitation occurs by (Eq 9) (Brown, 2011).

$$Mg^{2+}\ (aq) + HCO_3^-\ (aq) \leftrightarrow MgCO_3\ (aq) + H^+\ (aq) \quad \text{(Eq 6)}$$

$$Mg^{2+}\ (aq) + HCO_3^-\ (aq) + 3.2H_2O\ (l) \leftrightarrow 0.2\ Mg_5(CO_3)_4.Mg(OH)_2.4H_2O\ (s) + 0.2HCO_3^-\ (aq) + H^+\ (aq) \quad \text{(Eq 7)}$$

$$Mg^{2+}\ (aq) + HCO_3^-\ (aq) + 3H_2O\ (l) \leftrightarrow MgCO_3.3H_2O\ (s) + H^+\ (aq) \quad \text{(Eq 8)}$$

$$H_4SiO_4(aq) \leftrightarrow SiO_2(s) + 2H_2O\ (l) \quad \text{(Eq 9)}$$

Previously, our research team studied thermally activated serpentine dissolution without additives at ambient temperature with diluted CO_2 flue gas (18%) in a 300 mL pressurized batch reactor (11.5 bar total pressure). The leaching extent was limited by the solution equilibrium but successive leaching with fresh water allowed 50% Mg dissolution efficiency to be reached after six stages. Later on, pilot scale experiments operated in an 18.6 L batch reactor under 8 bar total pressure with real cement flue gas (18% CO_2) gave 18% Mg dissolution efficiency after three leaching stages (Kemache *et al.*, 2016; Pasquier *et al.*, 2014a). However, industrial gases are typically emitted continuously and are available at close to atmospheric pressure. Compressing the gas stream adds additional costs and CO_2 emissions. Consequently, this study aims to reduce the complexity and costs of mineral carbonation processes by considering continuous leaching operation of activated serpentine under atmospheric pressure with dilute CO_2 flue gas. A locally made bubble column reactor was used for this purpose. In addition, an attempt was made to understand the synergy between the CO_2 dissolution and activated serpentine dissolution based on observed reactions.

2 MATERIAL AND METHODS

2.1 Heat activated serpentine preparation

The material used in this work was the same as in our prior work and originated from residues of the Jeffrey mine situated in southern Quebec. The detailed preparation procedure is given with more details by (Kemache *et al.*, 2016). Essentially, this included magnetic separation, material grinding and thermal activation. A spiral (model 5LL400) followed by a wilfley table (Outokumpu Technology, model SA-13A) were used to remove the magnetic part to avoid the formation of a passivation layer during the heat activation. The material was then ground with a disc mill (Retsch Rs-2000) and thermally activated in an electric rotary kiln (Pyromaître Pyro 106-HE) at 650°C for 30 min. Heat activation time and temperature were chosen according to previously optimised conditions (Li *et al.*, 2009). Its final composition is reported in Table 1. It can be seen that the material composition is mainly Mg and Si with some impurities.

Table 1 Material composition after activation as reported by (Kemache *et al.*, 2016)

Elements	Units	Values
Al_2O_3	mg/g	1.33
CaO	mg/g	0.74
Cr_2O_3	mg/g	0.31
Fe_2O_3	mg/g	7.09
K_2O	mg/g	0.15
MgO	mg/g	47.62
MnO	mg/g	0.12
SiO_2	mg/g	47.11
TiO_2	mg/g	0.04
LOI*	wt	9

* Loss on ignition

2.2 Experimental setup and analytics

The experimental set up is illustrated in Figure 1. The column is made from Plexiglas and has an internal diameter of 5 cm and measures 102 cm high. It has a toroidal base where the gas is admitted and a flat head where the gas is removed at ambient pressure. The diffuser has an average pore size of 100 µm and is 4 cm in diameter. It is fixed 5 cm above the column base within a plastic frame that is flush with the column walls. A hole in the column head connects the agitation shaft with a magnetically coupled stirrer drive (Parr reactor 4555 series from Parr Company Inc). The drive is connected to a control system (Parr 4848M) which adjusts the power supply. The agitation speed is calibrated using a DivineXt DT-2234C+ tachymeter. The agitation shaft is made from stainless steel and two sets of impellers are used: a marine impeller and Rushton impellers. The marine impeller is placed 4 cm above the diffuser to disperse solid particles and prevent them from settling on the diffuser. The Rushton impellers are placed above to induce gas bubble breakage. The distance between each impeller is 14 cm. The column is equipped with four baffles to avoid vortexing, made in a single skeleton from stainless steel. A valve is fixed into the column cylinder to allow addition of serpentine slurry and sample collecting (C-valve, Figure 1).

The certified simulated CO_2 flue gas was provided from Linde with a volume composition of 4 % O_2, 18.2 % CO_2 balanced with N_2. Pure N_2 was also provided from Linde. A high precision mass flowmeter was used to control the amount of dilute CO_2 injected (SMART-TRAK 100). An analogue mass flowmeter (PMR1-010280) was used for N_2. The CO_2 content of the exit flue gas was continually measured with a 906 model Quantek Instruments CO_2 gas phase analyzer, with an accuracy of 2% of the measurement. A data logger (HOBO UX120-006M) was connected to the gas analyzer and to a computer to record data every 4 seconds.

In a typical experiment, the required amount of solid was weighed and mixed with 1 L of distilled water. N_2 was supplied to the column and agitation initiated. The C-valve was opened and a pump (MasterFlex 7528-10) was used to feed the prepared slurry into the column. Once the slurry was totally transferred, the pump was turned off and disconnected from the column and the C-valve closed. The gas supply was switched from N_2 to CO_2 at the desired flowrate (Figure 1) and data logging initiated. Samples were taken regularly with a syringe inserted into the C-valve. These samples were filtered using 25 µm filter paper and the pH of the liquid phase measured using a pH meter (Thermo Scientific Orien Star A111). ICP-AES analysis (Inductively

Coupled Plasma- Atomic Emission Spectroscopy, Vista AX CCO Simultaneous, Palo Alto, CA, USA) was used to determine the Mg and Si concentration in the liquid and dissolved CO_2 using a Total Organic Carbon analyzer (Shimadzu TOC-VCSH). At the end of the experiment, the CO_2 valve was closed and the column opened to remove the slurry. The temperature of the system was not controlled but was stable at 21°C ± 1°C.

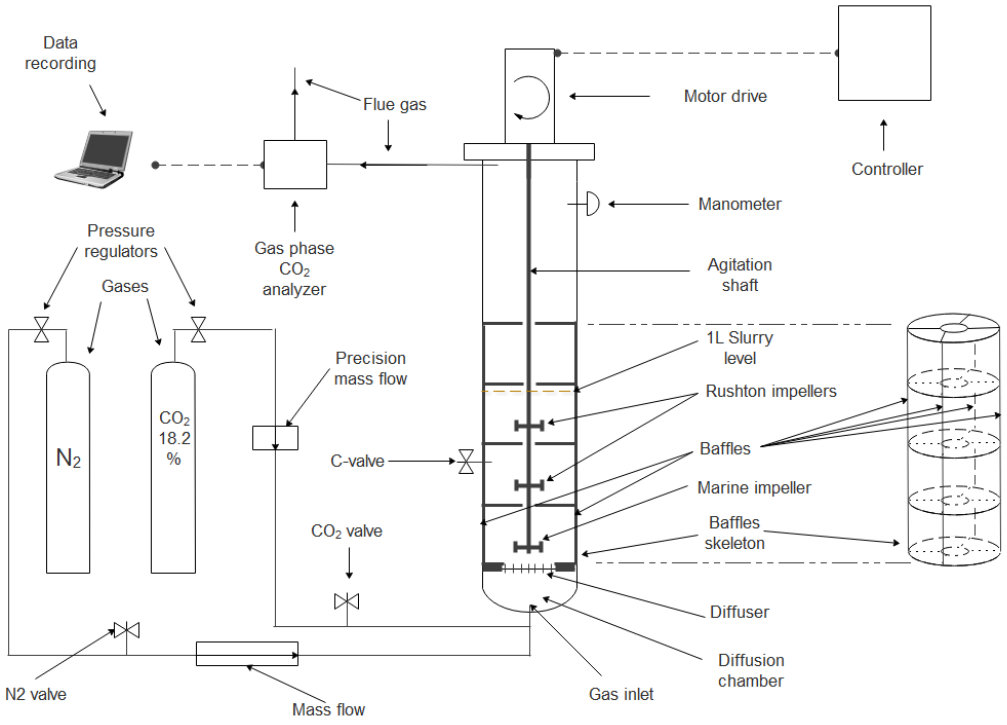

Figure 1 Experimental set up

2.3 Calculation

The outlet gas flowrate was calculated according to (Eq 11) which was obtained after performing a mass balance on the inert fraction in gas phase (Eq 10):

$$G^{out}(1 - y^{out}) = G^{in}(1 - y^{in}) \quad \text{(Eq 10)}$$

$$G^{out} = G^{in}(1 - y^{in})/(1 - y^{out}) \quad \text{(Eq 11)}$$

Where:

G^{in}: inlet gas flow (mL/min)

G^{out}: outlet gas flow (mL/min)

y^{in}: CO_2 volume fraction in the inlet gas

y^{out}: CO_2 volume fraction in the outlet gas

The CO_2 absorption ratio, which is the proportion of the CO_2 that is transferred to the solution, was estimated according to (Eq 12):

$$CO_2\text{absorption ratio} = (G^{in}.y^{in} - G^{out}.y^{out})/(y^{in}.G^{in}) \quad \text{(Eq 12)}$$

In this study, magnesium is more likely to precipitate as nesquehonite (Hänchen *et al.*, 2008). Its theoretical solubility is estimated as a function of the CO_2 partial pressure in the gas phase (Kline, 1929) while that for Si is considered constant (Chan, 1989).

The experimental error in Mg concentration was estimated using the differentiation method and was found to be around 4-5% of the measured value. Errors in the dissolved CO_2 concentration varied from 2-4% of the measured value. The inlet gas phase CO_2 concentration was certified by the manufacturer to be 2% of the specification. The error on the precision mass flowmeter was ± 12.5 mL/min regardless of flowrate. Therefore, the lower the flow, the higher the error. The differentiation method indicated an error of 1.2 to 7.5% across the flowrate range used here.

3 RESULTS AND DISCUSSION

3.1 Activated serpentine general leaching behavior

Typical experimental results are shown in Figure 2. The introduction of serpentine into the solution leads to an essentially instantaneous rise of the pH up to 10.3 (Figure 2e). Feng (2013) has shown that this is related to the initial leaching of residual hydroxyl groups from the heat activation step to form hydroxide ions in solution, leaving a layer enriched in magnesium and with a net positive charge on the serpentine surface. This Mg rich surface facilitates the leaching during the early reaction period (Feng *et al.*, 2013). Note that the activated serpentine used in this work was not completely dehydroxylated and still contained 35% residual water.

Even early in the reaction period, Mg dissolves at four times the rate of Si (Figure 2a and 2b). For example, after 5 minutes reaction time, the concentration of Mg and Si in the solution are respectively 15.6 and 3.7 mMol/L (Figure 2a and 2b). According to the literature, such incongruent dissolution is typical for serpentine and silicate minerals in general (Luce *et al.*, 1972) and relates to the much higher equilibrium solubility of Mg ions in the solution over silicate ions (Figure 2a and 2b). Indeed, the Si initially dissolved in the first minutes of reaction soon re-precipitates to reach its equilibrium solubility (< 100 mg/L) (Eq 9) (Figure 2b). The re-precipitation of silica (Eq 9) forms an additional diffusion barrier at the particle surface that increases with reaction time. This resistance contributes to the slowing magnesium dissolution, which is believed to be mass transfer controlled after the brief initial stage (Casey *et al.*, 1993; Crundwell, 2014; Schulze *et al.*, 2004) (figure 2a).

Figure 2f shows that the partial pressure of CO_2 in the exit gas is initially zero, but then increases gradually to reach an equilibrium value. As the CO_2 dissolves, the pH falls to reach a stable value around 8 (Eq. 3-5). This buffering behaviour is typical in serpentine dissolution under flue gas conditions (Werner *et al.*, 2014a). Nevertheless, it is believed to play an important role in improving the CO_2 absorption as CO_2 solubility is enhanced at high pH values (Pasquier *et al.*, 2014b; Wang *et al.*, 2010).

Figure 2c shows that the amount of CO_2 dissolved in the liquid phase (based on TOC analysis) is less than the amount absorbed (by gas phase measurement). This suggests that carbonate precipitation occurs simultaneously. Very similar behaviour was observed by other authors

(Pasquier *et al.*, 2014a; Werner *et al.*, 2014a). Nesquehonite formation (Eq 9) is favoured by its very small heterogeneous induction time at small supersaturation ratios (Cheng & Li, 2010). Hence, precipitation may lead to carbonates depositing on the mineral surface resulting in an extra diffusion barrier for the Mg atoms.

The Mg concentration initially increases with time and then declines after an hour of reaction time. This reflects dissolution being the dominant process in this first hour, while re-precipitation as magnesium carbonate becomes dominant at later timeframes, causing the Mg solubility to regress towards the equilibrium value. On the other hand, the CO_2 absorption continues to increase beyond the one hour mark, albeit at a slower rate. This is due to the uptake of CO_2 within the precipitated magnesium carbonate (Moreno Correia, 2018). This precipitation inside the reactor is undesirable, as carbonates can be covered at high purity for sale in a downstream reactor (Pasquier *et al.*, 2016). While the Mg concentration stabilizes at around 119 mMol/L after 60 minutes reaction time (Figure 2a), the Mg precipitated increases from 73 to 209 mMol/L (as obtained from Figure 2c). These results suggest that dissolution can be maximised and precipitation reduced by limiting the reactor residence time for the serpentine under these reaction conditions.

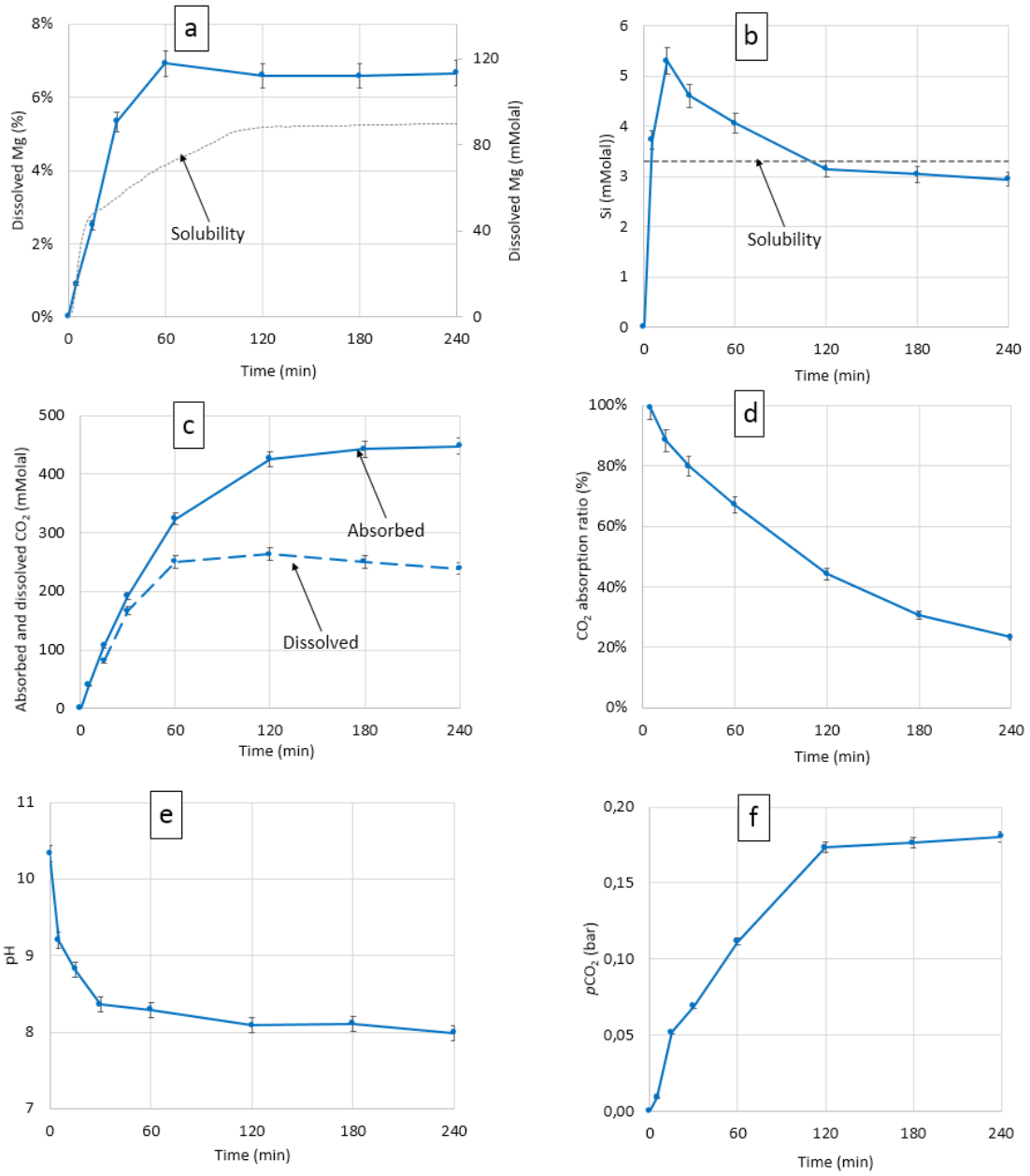

Figure 2 Dissolution behaviour of activated serpentine with diluted CO_2 flue gas (18.2% v/v) under ambient temperature and an atmospheric pressure, with 15 wt% solids concentration, 1000 mL/min gas flow and 600 RPM agitation speed. The dashed lines in (a) and (b) show the theoretical solubility of Mg and Si in water under these conditions, taken from (Chan, 1989) (Kline, 1929).

3.2 Effect of agitation

In industry, slurry bubble columns are generally operated at superficial gas velocities >0.4 m/s to avoid the need for mechanical agitation of the slurry phase (Krishna & Sie, 2000; Lefebvre, 2001). Under these conditions, the slurry is well mixed, but small bubbles coalesce to form bigger ones (Krishna & Sie, 2000) and this limits gas phase mass transfer, often requiring the gas phase to be recycled (Maretto & Krishna, 1999). In our case, it was technically complicated to operate a gas recycling system and thus lower superficial velocities (less than 0.02 cm/s) were used to allow for higher CO_2 absorption rates. Agitation was then required to enhance the mixing of the slurry phase. Initial tests indicated that the minimum agitation speed for which the solids did not settle to the bottom of the column was 300 RPM.

For a given reaction time, increasing the agitation speed beyond 300 RPM affected the amount of CO_2 absorbed to the solution especially between 300 and 600 RPM (Figure 3b). The Rushton blades break larger bubbles, increasing the interfacial area and resulting in improved mass transfer (Kazim, 2012; Martín *et al.*, 2008). Hence, this accelerates the CO_2 absorption rate. In serpentine mineral carbonation, most authors indicate that it is the mass transfer of magnesium to the surface of the serpentine particle that is rate controlling (Schulze *et al.*, 2004; Teir *et al.*, 2007). However, these results suggest that mass transfer of CO_2 from the gas to liquid phase is also important (Figure 3). There is a broad agreement in the literature that the H^+ concentration in solution, is the most important factor behind serpentine and activated serpentine dissolution (Alexander *et al.*, 2007; Farhang *et al.*, 2017; Werner *et al.*, 2014a). Given the high pH in the present experiments, H^+ equilibrium concentrations are extremely low. These ions only occur as transient species during the CO_2 dissolution into the liquid phase. Consequently and for a given reaction time, accelerating the CO_2 mass transfer increases the transient concentration of H^+ and thus improves the mineral dissolution rate.

Beyond 600 RPM any further increase of agitation provides only limited enhancement in Mg dissolution. Nevertheless, it also seems that increasing agitation speeds increase the carbonate precipitation rate, with an earlier decline in both Mg and dissolved CO_2 concentrations (Figure 3a and 3b).

As indicated in the introduction, the nesquehonite is the form of carbonates that precipitates under the reaction condition. According to (Eq 8), nesquehonite formation leads to the generation of H^+ species, which move the equilibrium towards the gaseous CO_2 formation (Eq 3-5). Hence, the higher the agitation, the higher the precipitation rate and the higher the CO_2 degassing. This is in accordance with previously observed results (Correia *et al.*, 2016). Still, the CO_2 is continuously fed to the solution. This is why the amount of CO_2 absorbed seems to move towards a stable value at the end of the reaction for all the agitation speeds (Figure 2b). This explains why the effect of agitation speed on the amount of CO_2 absorbed diminishes as long as the reaction proceeds (Figure 2b). Still, three hours of reaction time are required at 300 RPM to reach a similar level of dissolved Mg reached after only 1 hour for higher agitation speeds. Besides, at all agitator speeds, a similar supersaturation level is achieved. From these results, it was decided to fix the agitation at 600 RPM for the rest of the study, as this provides the same results in a shorter reaction time.

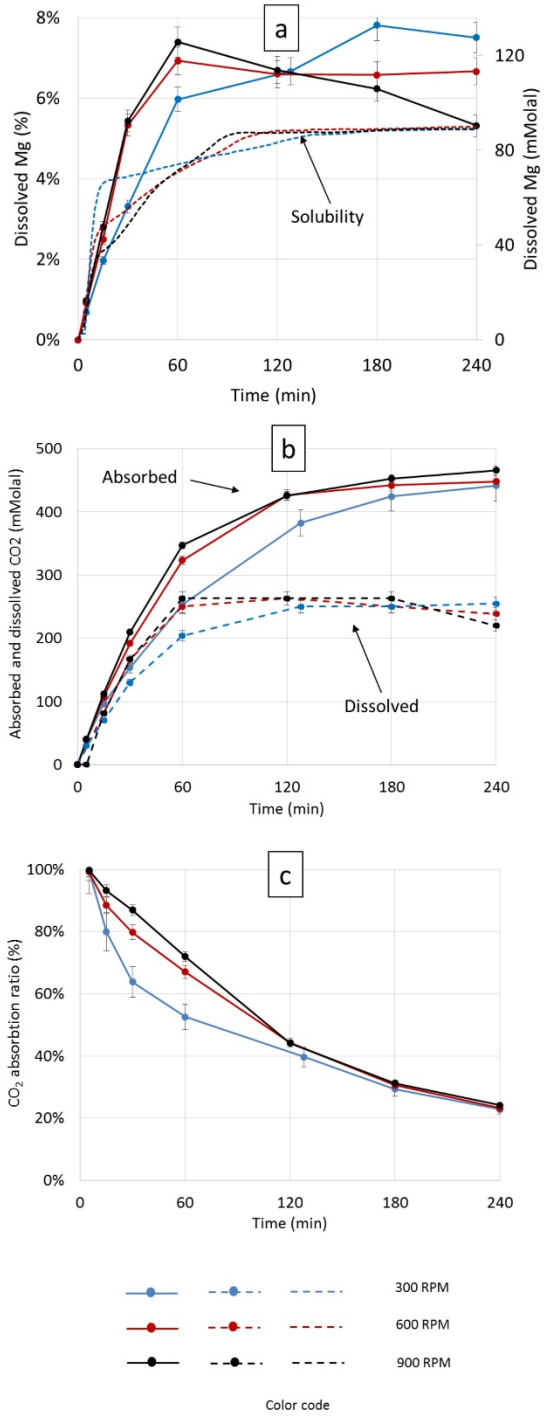

Figure 3 Effect of agitation on serpentine leaching (solids concentration = 15 wt%, flue gas flowrate = 1000 mL/min)

3.3 Effect of solid concentration and gas flow

Higher superficial gas velocities (gas flowrates) lead to faster Mg leaching and CO_2 absorption (all figures 4a and 4b). However, increasing the gas flow also leads to a sharper and earlier decrease in dissolved Mg and CO_2, suggesting faster precipitation kinetics (Eq 8). Similar evidence of enhanced precipitation at higher gas flowrates is obtained comparing the CO_2 absorption and concentration curves (all figures 4a and 4b). The reduction of Mg concentration occurs at the same time point as the reduction of the dissolved CO_2 in solution indicating carbonate formation.

For a given reaction time, the increase in gas flow increased the rate of CO_2 absorption (Figures 4b) by increasing the gas hold up, which is the volume fraction of the gas present in the solution (Krishna & Sie, 2000). This increase in holdup with gas flowrate was validated for our system by a broth surface height method (Hofmeester, 1988). Several authors have demonstrated that the mass transfer is linearly proportional to the gas hold up (Krishna *et al.*, 1999; Letzel *et al.*, 1999; Plais *et al.*, 2005; Vandu & Krishna, 2003) as the greater population of bubbles result in an increased gas/liquid interfacial area. As discussed earlier, this leads to higher transient concentrations of H^+ improving mineral leaching. Nevertheless, increasing the gas flow leads to a decrease in CO_2 absorption efficacy (Figure 4c) and a decrease in the maximum concentration of absorbed CO_2 (Figure 4a). This means that the improved mass transfer resulting from the higher gas superficial velocity was not enough to overcome the reduced residence time of the gas in the column at these higher flowrates. Note that the amount of CO_2 absorbed decreases after it reaches a maximum for the gas flow 2500 mL/min (All Figures 4 b). As indicated in section 3.2, the precipitation is accompanied with a degassing effect. For this high gas flow, the solution saturates fast and the degassing effect starts earlier.

Increasing the solid concentration decreases the proportion of dissolved Mg (Figure 4a). This means that Mg transfer from the solid surface to the bulk solution is the rate controlling for the reaction kinetics. Similar conclusion were drawn elsewhere regarding mineral silicate dissolution (Huijgen *et al.*, 2006; Luce *et al.*, 1972; Wang & Maroto-Valer, 2011). One way to overcome this system inefficiency is to operate successive leaching of the same solid with fresh water. Successive leaching with solution renewal is a well-established technique used in extraction processes including mineral leaching (Coulson *et al.*, 1991). This has also been proven effective

in serpentine leaching in our earlier work (Pasquier *et al.*, 2014a). These results are presented in the following Section.

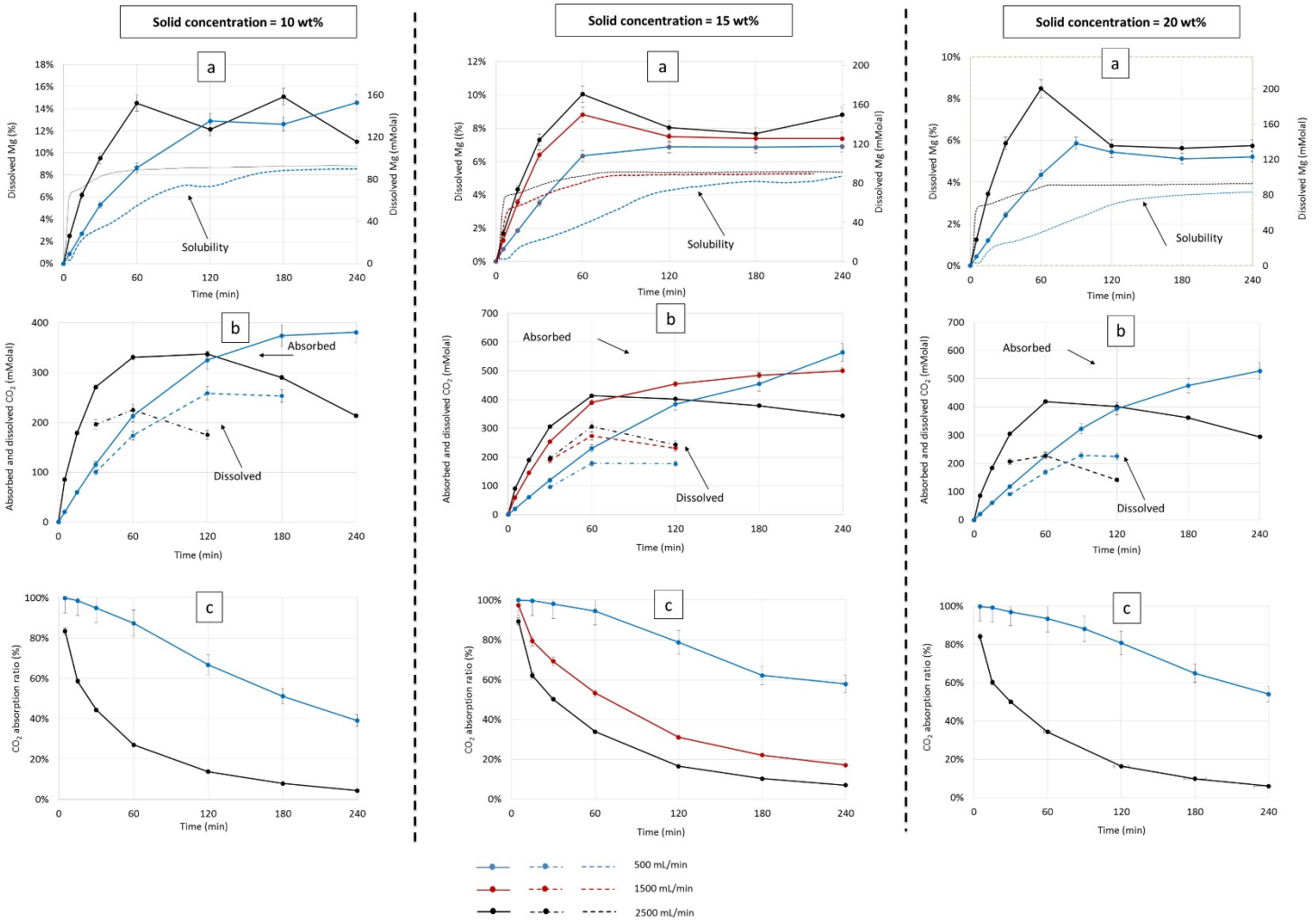
Solid concentration = 10 wt%
Solid concentration = 15 wt%
Solid concentration = 20 wt%
a
b
c
Dissolved Mg (%)
Dissolved Mg (mMolal)
Solubility
Time (min)
Absorbed and dissolved CO2 (mMolal)
Absorbed
Dissolved
CO2 absorption ratio (%)
500 mL/min
1500 mL/min
2500 mL/min

Figure 4 The effect of solids concentration and gas flowrate on serpentine leaching behaviour with simulated flue gas and 600 RPM agitation speed

3.4 Successive leaching

From the previous results, it appears that beyond 2 h reaction time, the concentration of dissolved Mg does not improve under any conditions, with precipitation becoming dominant. The CO_2 absorption ratio is similarly affected. We have previously shown that this restriction can be overcome through the use of successive leaching steps (Pasquier *et al.*, 2014a).

In the present case, we compare these earlier results in a batch reactor (Purple bars in Figure 5) with the use of successive batches in the bubble column. Conditions in the earlier study were optimized for six leaching stages of 30 minutes each with a solid concentration of 15% under ambient temperature and 10.5 bar gauge pressure with two batches of gas (18.2% CO2 on a volume basis) for each stage (15 minutes each) and an intermediate grinding after the third leaching stage. Note that the material used in this previous study originated from a different source (Thetford mines) and was processed in smaller quantities (Pasquier *et al.*, 2014a). This experiment was also performed here with the material used in this work (Black bars in Figure 5). Conditions in the column of 500 mL/min gas flow and 10% solids concentration were used, as after 2 h of reaction, this gave 67 % CO_2 absorption and 12.9 % Mg dissolved, which is similar to the first leaching stage of the previous study. Six successive leaching stages were again used. In one experiment there was an intermediate grinding after the third leaching stage (Blue bars in Figure 5), while in the other a systematic intermediate grinding was use after each leaching stage (Red bars in Figure 5).

Figure 5 confirms that successive leaching was effective in increasing the dissolvable Mg by overcoming the equilibrium limitations. Werner (2014a) similarly showed that removing dissolved Mg from the solution improved serpentine leaching. The Figure also shows that the mineral reactivity declines across the successive stages. While intermediate grinding was shown previously to reactivate the material (Pasquier *et al.*, 2014a), in the present case it did not seem to improve the leaching at the following stage suggesting that, in addition to material passivation, Mg depletion in the surface layer is also affecting the material reactivity. When intermediate grinding was applied only after the third stage (Red bars in Figure 5), the reactivation was more noticeable. Further, this single grinding had the same effect on the cumulative Mg depletion as when five successive grinds were used. This indicates that the

passivation layer forms gradually (Schulze *et al.*, 2004) so that repetitive grinding adds little value.

The total cumulative Mg recovered within the liquid was 32% in the bubble column for both protocols compared to 33% obtained in the batch reactor under 11.5 bar. The large difference in operating pressure did not seem to have an impact on the total amount of recovered Mg for the material used in this study. In our previous study under 11.5 bar, the amount of Mg recovered was 50% (Purple bars in Figure 5). The material in this earlier work originated from another mine and the activation was performed on a smaller scale and in a different kiln.

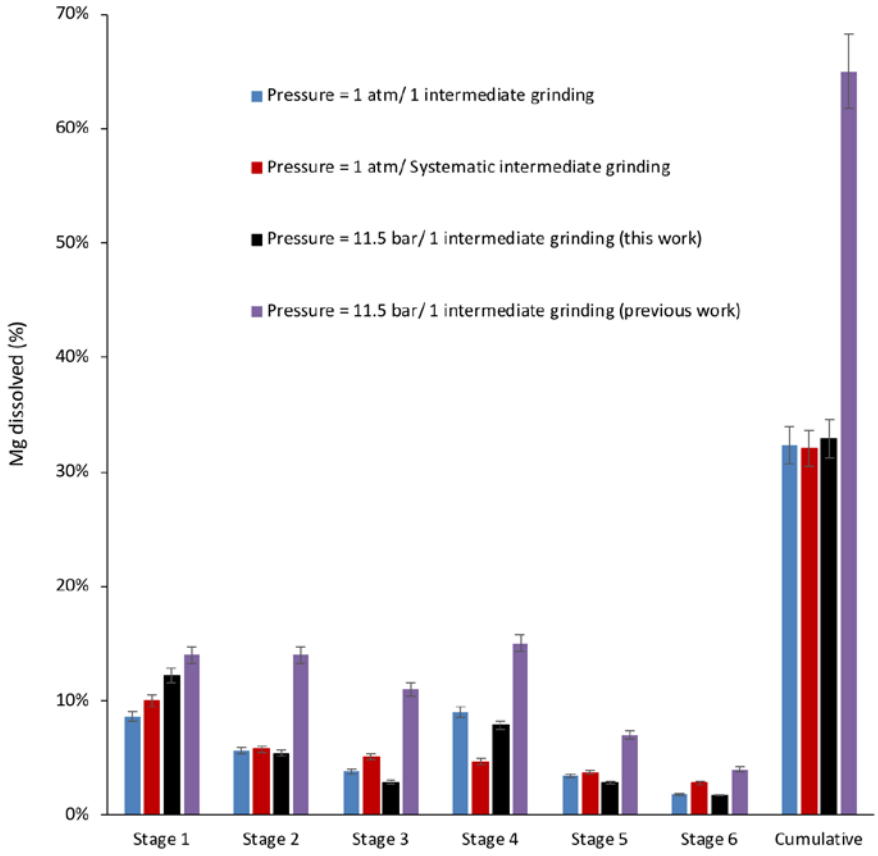

Figure 5 Results of the six leaching stages for the same material with different protocols. The first two bars refer to the use of the bubble column at 1 atm total pressure, ambient temperature, 500 ml/min gas flow and 10% solids concentration. The second two bars refer to the use of a batch reactor at 11.5 atm total pressure, ambient temperature, two batches of gas of 15 minutes each with 10.5 bar gauge pressure of gas and 15 % solids concentration.

3.5 Insight into activated serpentine leaching mechanism under CO_2 flue gas conditions

This section attempts to give some insights into the mechanism behind the leaching of thermally activated serpentine under CO_2 flue gas conditions. In general, the leaching of serpentine and other magnesium silicates is known to be dependent on the H^+ activity in both acid and alkaline conditions (Bales & Morgan, 1985; Daval *et al.*, 2013). The reaction order in regards to H^+ activity generally shifts from 0.5 under acid conditions to 0.25 under alkaline to neutral conditions (Bales & Morgan, 1985; Crundwell, 2014; Daval *et al.*, 2013). Crundwell (2014) attributed the change in the reaction order to the change in the reaction location. Under acidic conditions (pH < 6), H^+ ions are in abundance and react with the departing SiO_4^{4-} group to form an activated complex of $HSiO_3^{3-}$ at the outer Helmholtz plane in a reaction of order 0.5, while the metal atoms react with water to form solvated cations. Conversely, under alkaline to neutral conditions, the H^+ are scarce in the solution and are first adsorbed at the inner Helmholtz layer before reacting with the mineral to form the activated $HSiO_3^{3-}$complex at this inner location (Crundwell, 2014). This specific adsorption of H^+ to the mineral surface is first order and thus alters the overall reaction order (Crundwell, 2014). Meanwhile, the metal atoms react with hydroxide ions form hydrolyzed cations. In this work, the mechanism used to describe activated serpentine leaching is based on that reported by Crundwell under alkaline conditions that assumes that the magnesium silicate leaching occurs through the attack of H_2O molecules on the brucite group $[Mg_3O_2(OH)_4]^{2-}$ while the silicate group $[SiO_4]^{4-}$ is attacked by H^+ ions.

When activated serpentine is dissolved in water in the absence of CO_2, there is an initial very rapid increase in solution pH related to the loss of hydroxyl groups from the surface leading to a net positive surface charge, as discussed earlier. On the other hand, when CO_2 is bubbled in water in the absence of serpentine, the pH falls (pH ≈4 after few minutes) due to (Eq 3-5), which subsequently reduces further CO_2 uptake (Kern, 1960). In simultaneous leaching, the pH is buffered at around 8 (Figure 6). In this case, the CO_2 is mainly present in the bicarbonate form with approximately one molecule H^+ generated for each CO_2 absorbed (Eq 5). A mass balance revealed that a large amount of H^+ is liberated from this reaction. For example, after 30 min only, this is higher than 0.1 mol/L. Were this H^+ not consumed, the pH of the solution would fall to a value lower than 1. However, in this first reaction period, the H^+ is consumed by reacting with SiO_4^{4-}, which in turn, cause both Mg and CO_2 (Eq 3-5) to dissolve further. After around one

hour, the pH stabilises due the fact that no further silica can dissolve. That is, the silica concentration in the solution has reached (or exceeded) its equilibrium value. This prohibits the leaching of any further silica, which in turn significantly affects the ability of Mg to dissolve, as it must now diffuse through a silica-rich layer on the solid surface. Surface grinding can remove some of this silica surface layer, but in the present case, this grinding is of little effect.

Figure 6 illustrates serpentine and CO_2 dissolution with respect to time for the experiment with 500 mL/min gas flow, 10% w/w solids concentration and 600 RPM agitation speed. Both pH and the corresponding pCO_2 are indicated on the figure. The CO_2 equilibrium solubility in the absence of serpentine, which is the sum of total dissolved CO_2, H_2CO_3, HCO_3^-, and CO_3^{2-} is calculated according to (Eq 13) using equilibrium data as taken from (Chen *et al.*, 2006).

$$Total\ dissolved\ CO_2 = \frac{1}{K_H}\left[p_{CO_2} + K_{HCO_3^-}\frac{p_{CO_2}}{10^{-pH}} + K_{CO_3^{2-}}K_{HCO_3^-}\frac{p_{CO_2}}{\left(10^{-pH}\right)^2} \right] \quad \text{(Eq 13)}$$

Where:

K_H is the henry constant for CO_2 at 25°C = 29.4 atm/(mol.L)

H_{CO3-} is the equilibrium constant of the system $H_2CO_3/HCO3^-$ = 4.5 10^{-7} as taken from

K_{CO3-2} is the equilibrium constant of the system HCO_{3-}/CO_3^{2-} = 4.7*10^{-11} as taken from

Note that the CO_2 solubility depends on both pH and p_{CO2}, which is why it increases when the pH decreases (Figure 6). Figure 6 indicates that the amount of dissolved CO_2 in the presence of activated serpentine (grey bars) is less than the equilibrium solubility calculated in the absence of this material (solid black line). Both values increase with time to reach a maximum when the pH and p_{CO2} reach equilibrium. H^+ consumption via mineral leaching increases the CO_2 solubility in the system, which promotes further CO_2 absorption. This mechanism is similar to that proposed by (Donaldson & Nguyen, 1980) for CO_2 absorption in tertiary amine solutions or to that proposed by (Back *et al.*, 2011) for bauxite leaching in the presence of CO_2. Hence, improved CO_2 absorption results in additional H^+ generation which enhances the silica leaching as discussed earlier. Therefore, a synergistic effect between the two reactions emerges from their opposing behaviour to the H^+ in solution. Nevertheless, additional work must be carried to

clearly understand the fate of H^+ which would give further understanding of the mechanism behind serpentine leaching in the presence of CO_2.

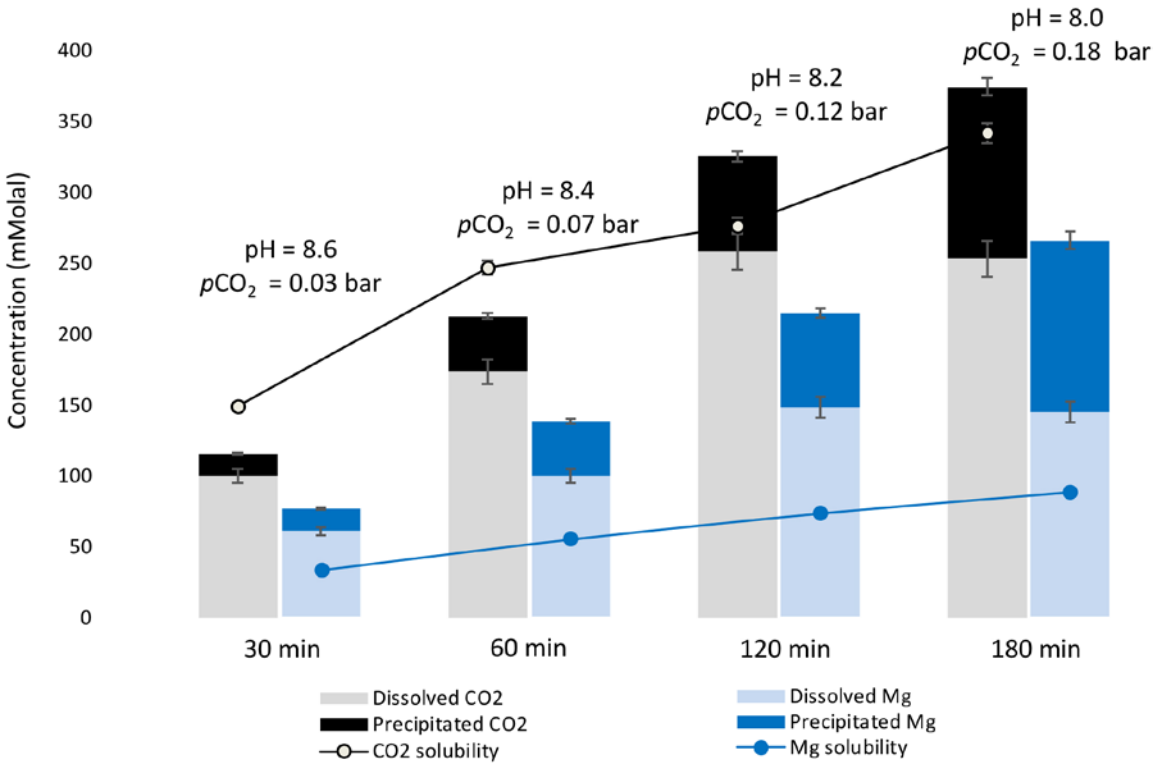

Figure 6 Highlighting of the synergy effect between serpentine leaching and CO_2 absorption. 500 mL/min gas flow, 10% w/w solids concentration and 600 RPM agitation speed

4 CONCLUSION

This study aimed to demonstrate the feasibility of activated serpentine leaching under ambient temperature and atmospheric pressure directly with dilute flue gas. The flue gas contained 18.2% CO_2 on a volume basis, which is typical for cement flue gases. The reaction was performed in a 2 L bubble column reactor operated in a homogeneous regime. 1 L slurry was used for each experiment. Agitation was required to provide sufficient mixing and was varied from 300 to 900 RPM. Solid concentration was varied from 10 to 20 wt% and the gas flow from 500 to 2500 mL/min. CO_2 analysis of the outlet flue gas allowed us to estimate the CO_2 absorption ratio while liquid sampling was performed to obtain the dissolved Mg and CO_2. The quantity of precipitated carbonates was deduced from a mass balance on CO_2.

Precipitation was found to occur simultaneously with serpentine leaching as the Mg concentration moved toward and equilibrium regardless of the reaction conditions. In addition, increasing the solid concentration reduced the proportion of dissolved Mg which confirms that mass transfer is rate controlling. For the range of parameters studied here, it was found that reaction time must be limited to 2 hours. This is because after this period, the solution is saturated with silica, which in turn prevents further serpentine leaching. Beyond that, CO_2 absorption occurs only as a result of precipitation of magnesium carbonates. Successive leaching with fresh water was shown to overcome the equilibrium limitations, as 32% of the total Mg content of the material was dissolved. As a comparison, 33% of the same material content of Mg was dissolved when the reaction was operated according to previously optimized conditions in a batch reactor under 11.5 bar. This indicates that a pressurized medium is not mandatory for serpentine leaching with dilute CO_2 flue gas. Nevertheless, material reactivity declined along with the successive leaching stages. Systematic intermediate grinding after each leaching stage did not increase the total Mg dissolved but made the leaching more homogenous along the stages.

Increasing agitation and superficial gas velocity were found to increase the amount of dissolved CO_2. This was caused by the enhanced CO_2 mass transfer coefficient and increased interfacial area for mass transfer. This also accelerated the serpentine leaching as more transient H^+ were available from the absorbed CO_2 hydration reaction. Enhancement of CO_2 absorption in the

presence of serpentine was thermodynamically linked to H^+ consumption during serpentine leaching and a synergistic mechanism between both reactions was proposed.

This study highlights the feasibility of mineral carbonation under atmospheric pressure and ambient temperature. Eliminating the need for flue gas compression prior to usage in leaching reduces the costs and environmental burden. This facilitates retrofit issues for existing plants and improves the overall economics of the process.

Future work must focus on leaching under a heterogeneous bubble column regime to avoid the energy consumption related to agitation. Nevertheless, for higher CO_2 absorption ratios and limited precipitation, shorter residence times should be considered for each leaching stage. Two systems could be proposed for this operation: flue gas recycling or countercurrent gas-slurry leaching stages. Finally, more research needs to be done for a deeper understanding of the mechanism behind activated serpentine leaching with CO_2.

AKNOWLEDGMENTS

This work was financially supported by Les Fonds de recherche du Québec - Nature et technologies en équipe de 190542.

5 REFERENCES

Alexander G, Mercedes Maroto-Valer M & Gafarova-Aksoy P (2007) Evaluation of reaction variables in the dissolution of serpentine for mineral carbonation. *Fuel* 86(1):273-281.

Back M, Bauer M, Stanjek H & Peiffer S (2011) Sequestration of CO2 after reaction with alkaline earth metal oxides CaO and MgO. *Applied Geochemistry* 26(7):1097-1107.

Bales RC & Morgan JJ (1985) Dissolution kinetics of chrysotile at pH 7 to 10. *Geochimica et Cosmochimica Acta* 49(11):2281-2288.

Balucan R (2013) *Thermal Studies of magnesium silicates from the Great Serpentinite Belt in New South Wales for CO2 sequestration by mineral carbonation in Australia*. (The University of Newcaslte, Newcastle, Australia).

Balucan RD, Dlugogorski BZ, Kennedy EM, Belova IV & Murch GE (2013) Energy cost of heat activating serpentinites for CO2 storage by mineralisation. *International Journal of Greenhouse Gas Control* 17:225-239.

Brown K (2011) Thermodynamics and kinetics of silica scaling. in *Proceedings of International Workshop on Mineral Scaling in Geothermal Environment* Manila, Philippines), p 25-27.

Casey WH, Westrich HR, Banfield JF, Ferruzzi G & Arnold GW (1993) Leaching and reconstruction at the surfaces of dissolving chain-silicate minerals. *Nature* 366:253.

Chan SH (1989) A review on solubility and polymerization of silica. *Geothermics* 18(1):49-56.

Chen Z-Y, O'Connor WK & Gerdemann SJ (2006) Chemistry of aqueous mineral carbonation for carbon sequestration and explanation of experimental results. *Environmental Progress* 25(2):161-166.

Cheng W & Li Z (2010) Nucleation kinetics of nesquehonite (MgCO3·3H2O) in the MgCl2−Na2CO3 system. *Journal of Crystal Growth* 312(9):1563-1571.

Correia MJM, Pasquier LC, Blais JF, Illiuta M & Mercier G (2016) L'influence de la température sur la précipitation des carbonates de magnésium et son impact sur le bilan du carbone dans un procédé de séquestration de CO2. *Journée des Sciences de la Terre et de Environnement* (Quebec, Québec, Canada, 18 mars 2016).

Coulson JM, Richardson JF, Backhurst JR & Harker JH (1991) Leaching. *Particle technology and separation processes*, Elsevier (Édit.) Pergamon Press, Oxford, UK Vol 2. p 533-536.

Crundwell FK (2014) The mechanism of dissolution of minerals in acidic and alkaline solutions: Part II Application of a new theory to silicates, aluminosilicates and quartz. *Hydrometallurgy* 149:265-275.

Daval D, Hellmann R, Martinez I, Gangloff S & Guyot F (2013) Lizardite serpentine dissolution kinetics as a function of pH and temperature, including effects of elevated pCO2. *Chemical Geology* 351:245-256.

Dlugogorski BZ & Balucan RD (2014) Dehydroxylation of serpentine minerals: Implications for mineral carbonation. *Renewable and Sustainable Energy Reviews* 31:353-367.

Donaldson TL & Nguyen YN (1980) Carbon dioxide reaction kinetics and transport in aqueous amine membranes. *Industrial & Engineering Chemistry Fundamentals* 19(3):260-266.

Farhang F, Rayson M, Brent G, Hodgins T, Stockenhuber M & Kennedy E (2017) Insights into the dissolution kinetics of thermally activated serpentine for CO2 sequestration. *Chemical Engineering Journal* 330:1174-1186.

Feng B, Lu Y-p, Feng Q-m, Ding P & Luo N (2013) Mechanisms of surface charge development of serpentine mineral. *Transactions of Nonferrous Metals Society of China* 23(4):1123-1128.

Gerdemann SJ, O'Connor WK, Dahlin DC, Penner LR & Rush H (2007) Ex situ aqueous mineral carbonation. *Environmental Science & Technology* 41(7):2587-2593.

Goff F, Guthrie G, Lipin B, Fite M, Chipera S, Counce D, Kluk E & Ziock H (2000) Evaluation of ultramafic deposits in the Eastern United States and Puerto Rico as sources of magnesium for carbon dioxide sequestration. (Los Alamos National Lab., NM (US), New Mexcico, US), p 3.

Hänchen M, Prigiobbe V, Baciocchi R & Mazzotti M (2008) Precipitation in the Mg-carbonate system—effects of temperature and CO2 pressure. *Chemical Engineering Science* 63(4):1012-1028.

Hofmeester JJM (1988) Gas hold-up measurements in bioreactors. *Trends in Biotechnology* 6(1):19-22.

Huijgen WJJ, Witkamp G-J & Comans RNJ (2006) Mechanisms of aqueous wollastonite carbonation as a possible CO2 sequestration process. *Chemical Engineering Science* 61(13):4242-4251.

Kazim SA (2012) *Experimental & Empirical Correlations for the Determination of the Overall Volumetric Mass Transfer Coefficients of Carbon Dioxide in Stirred Tank Bioreactors*. M.E.Sc (The University of Western Ontario, London, Ontario, Canada). 48-54 p

Kemache N, Pasquier L-C, Mouedhen I, Cecchi E, Blais J-F & Mercier G (2016) Aqueous mineral carbonation of serpentinite on a pilot scale: The effect of liquid recirculation on CO2 sequestration and carbonate precipitation. *Applied Geochemistry* 67:21-29.

Kern DM (1960) The hydration of carbon dioxide. *Journal of Chemical Education* 37(1):14.

Kline WD (1929) THE SOLUBILITY OF MAGNESIUM CARBONATE (NESQUEHONITE) IN WATER AT 25° AND PRESSURES OF CARBON DIOXIDE UP TO ONE ATMOSPHERE1. *Journal of the American Chemical Society* 51(7):2093-2097.

Krishna R & Sie ST (2000) Design and scale-up of the Fischer–Tropsch bubble column slurry reactor. *Fuel Processing Technology* 64(1–3):73-105.

Krishna R, Urseanu MI, van Baten JM & Ellenberger J (1999) Rise velocity of a swarm of large gas bubbles in liquids. *Chemical Engineering Science* 54(2):171-183.

Lefebvre S (2001) *Caractérisation de l'hydrodynamique d'une colonne à bulles à l'aide de mesures locales*. Maitrise (Université de Montréal, Montréal, Québec, Canada). 5 p

Letzel HM, Schouten JC, Krishna R & van den Bleek CM (1999) Gas holdup and mass transfer in bubble column reactors operated at elevated pressure. *Chemical Engineering Science* 54(13–14):2237-2246.

Li J & Hitch M (2018) Mechanical activation of magnesium silicates for mineral carbonation, a review. *Minerals Engineering* 128:69-83.

Li W, Li W, Li B & Bai Z (2009) Electrolysis and heat pretreatment methods to promote CO2 sequestration by mineral carbonation. *Chemical Engineering Research and Design* 87(2):210-215.

Luce RW, Bartlett RW & Parks GA (1972) Dissolution kinetics of magnesium silicates. *Geochimica et Cosmochimica Acta* 36(1):35-50.

Maretto C & Krishna R (1999) Modelling of a bubble column slurry reactor for Fischer–Tropsch synthesis. *Catalysis Today* 52(2–3):279-289.

Martín M, Montes FJ & Galán MA (2008) Bubbling process in stirred tank reactors II: Agitator effect on the mass transfer rates. *Chemical Engineering Science* 63(12):3223-3234.

Moreno Correia M-J (2018) *Optimisation de la précipitation des carbonates de magnésium pour l'application dans un procédé de séquestration de co_2 par carbonatation minérale de la serpentine*. Maitrise (Université du Québec, Institut national de la recherche scientifique, Québec, Québec, Canada). 57-64 p

Olajire AA (2013) A review of mineral carbonation technology in sequestration of CO2. *Journal of Petroleum Science and Engineering* 109:364-392.

Pasquier L-C, Mercier G, Blais J-F, Cecchi E & Kentish S (2014a) Parameters optimization for direct flue gas CO2 capture and sequestration by aqueous mineral carbonation using activated serpentinite based mining residue. *Applied Geochemistry* 50:66-73.

Pasquier L-C, Mercier G, Blais J-F, Cecchi E & Kentish S (2014b) Reaction Mechanism for the Aqueous-Phase Mineral Carbonation of Heat-Activated Serpentine at Low Temperatures and Pressures in Flue Gas Conditions. *Environmental Science & Technology* 48(9):5163-5170.

Pasquier L-C, Mercier G, Blais J-F, Cecchi E & Kentish S (2016) Technical & economic evaluation of a mineral carbonation process using southern Québec mining wastes for CO2 sequestration of raw flue gas with by-product recovery. *International Journal of Greenhouse Gas Control* 50:147-157.

Plais C, Billet A-M, Julcour-Lebigue C & Delmas H (2005) Etude du transfert gaz-liquide en présence d'une troisième phase finement divisée. *Récents Progrès en Génie des Procédés, Numéro 92* 92(92).

Schulze RK, Hill MA, Field RD, Papin PA, Hanrahan RJ & Byler DD (2004) Characterization of carbonated serpentine using XPS and TEM. *Energy Conversion and Management* 45(20):3169-3179.

Seifritz W (1990) CO2 disposal by means of silicates. *Nature* 345:486.

Sipilä J, Teir S & Zevenhoven R (2008) Carbon dioxide sequestration by mineral carbonation: Literature review update 2005–2007. in *Report Vt 2008-1* (Åbo Akademi University, Turku, Finland), p 12.

Teir S, Revitzer H, Eloneva S, Fogelholm C-J & Zevenhoven R (2007) Dissolution of natural serpentinite in mineral and organic acids. *International Journal of Mineral Processing* 83(1):36-46.

Vandu CO & Krishna R (2003) Gas Holdup and Volumetric Mass Transfer Coefficient in a Slurry Bubble Column. *Chemical Engineering & Technology* 26(7):779-782.

Vitillo JG (2015) Magnesium-based systems for carbon dioxide capture, storage and recycling: from leaves to synthetic nanostructured materials. *RSC Advances* 5(46):36192-36239.

Wang X, Conway W, Burns R, McCann N & Maeder M (2010) Comprehensive Study of the Hydration and Dehydration Reactions of Carbon Dioxide in Aqueous Solution. *The Journal of Physical Chemistry A* 114(4):1734-1740.

Wang X & Maroto-Valer MM (2011) Dissolution of serpentine using recyclable ammonium salts for CO2 mineral carbonation. *Fuel* 90(3):1229-1237.

Werner M, Hariharan S & Mazzotti M (2014a) Flue gas CO2 mineralization using thermally activated serpentine: from single- to double-step carbonation. *Physical Chemistry Chemical Physics* 16(45):24978-24993.

Werner M, Hariharan S, Zingaretti D, Baciocchi R & Mazzotti M (2014b) Dissolution of dehydroxylated lizardite at flue gas conditions: I. Experimental study. *Chemical Engineering Journal* 241:301-313.